

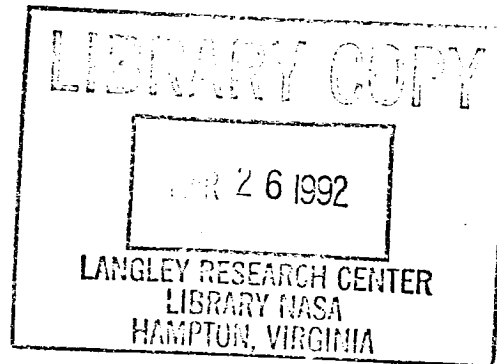
NASA Technical Memorandum 104215

NASA-TM-104215 19920011238

**QUALITY ASSESSMENT OF TWO- AND THREE-
DIMENSIONAL UNSTRUCTURED MESHES AND
VALIDATION OF AN UPWIND EULER FLOW SOLVER**

**PAUL R. WOODARD
JOHN T. BATINA
HENRY T. Y. YANG**

FEBRUARY 1992



**National Aeronautics and
Space Administration**

**Langley Research Center
Hampton, Virginia 23665**

QUALITY ASSESSMENT OF TWO- AND THREE-DIMENSIONAL UNSTRUCTURED MESHES AND VALIDATION OF AN UPWIND EULER FLOW SOLVER

Paul R. Woodard*
Purdue University
West Lafayette, Indiana 47907

John T. Batina†
NASA Langley Research Center
Hampton, Virginia 23665-5225

Henry T. Y. Yang‡
Purdue University
West Lafayette, Indiana 47907

Abstract

Quality assessment procedures are described for two-dimensional and three-dimensional unstructured meshes. The procedures include measurement of minimum angles, element aspect ratios, stretching, and element skewness. Meshes about the ONERA M6 wing and the Boeing 747 transport configuration are generated using an advancing front method grid generation package of programs. Solutions of Euler's equations for these meshes are obtained at low angle-of-attack, transonic conditions. Results for these cases, obtained as part of a validation study demonstrate accuracy of an implicit upwind Euler solution algorithm.

Introduction

In recent years, considerable progress has been made in developing computational fluid dynamics (CFD) methods for unstructured triangular and tetrahedral meshes[1-9]. These meshes are an alternative to the traditional structured meshes, for which many CFD algorithms have been developed. Unstructured meshes have several distinct advantages over their structured mesh counterparts. For example, they can treat arbitrary complex geometries effectively, and they readily lend themselves to spatial adaption procedures. These advantages result from the arbitrary nature of the numbering and placement of the nodes and elements which make up a mesh.

The generation of unstructured meshes generally falls into three broad categories, which are the triangularization of structured grids, Voronoi/Delaunay triangularization[10-13], and the advancing front method[4, 14, 15]. The simplest of

these methods is the triangularization of an already generated structured grid. While this method is quick, it does not effectively make use of the inherent advantages of unstructured grids. Voronoi/Delaunay triangularization requires that the nodes that are used to make up a mesh already are distributed. This method then takes the nodes and connects them to form unstructured meshes. In contrast, the advancing front method does not require any point or segment distribution, but rather generates the required points as it creates the mesh. Because of this, it shows the most promise of the unstructured grid generation methods for future development.

Despite the advances of grid generation methods, a significant drawback in unstructured grid technology is the lack of effective grid quality measures. With meshes for realistic three-dimensional configurations having a quarter million or more elements, the computer time required to solve the flow equations on one of these meshes is relatively large. Because problems in these meshes can effect the solution time and accuracy significantly, it becomes important to be able to assess the quality of a mesh before many hours of computer time are used in an attempt to obtain a solution on a mesh of questionable quality.

To assess the state of unstructured mesh grid generation, two advancing front method grid generation packages of programs were used in the present study, and several measures were created to determine mesh quality. Meshes were generated about the ONERA M6 wing and about the Boeing 747 transport configuration. The purpose of this paper is to report the quality evaluations that were performed for these meshes and to present numerical solutions of the Euler equations that are determined on these meshes. Steady flow results are calculated on these meshes and are compared to experimental data as part of a validation study of a three-dimensional implicit upwind Euler solution algorithm.

Advancing Front Method

In the two-dimensional advancing front method, elements are generated by marching a "front" of free sides into the computational domain. The initial front is created by

*Graduate Research Assistant, School of Aeronautics and Astronautics, Member AIAA.

†Senior Research Scientist, Unsteady Aerodynamics Branch, Structural Dynamics Division, Senior Member AIAA.

‡Professor and Dean, Schools of Engineering, Fellow AIAA.

subdividing the prescribed boundary segments according to the spacing determined by interpolation from a background grid, an example of which is shown in figure 1(a). New triangles are created by extending this front, also according to the background spacing. If possible an existing node is used to generate this new element, but, if necessary, a new node is created. Once a new element has been created, the front is updated to reflect changes due to the creation of the new element, as shown in figure 1(b). This procedure continues until all sides in the front are removed, and the domain is meshed, as shown in figure 1(c).

The method works similarly in three dimensions. The initial front is composed of a surface mesh of triangles. This surface mesh is created by applying the two-dimensional grid generator to surface regions which are specified by taking convenient subsets of the entire boundary. These regions first must be mapped to a two-dimensional computational space, then back to three dimensions once a region is meshed. From this front, a triangular side is chosen to create a new element. A new tetrahedron is formed, using either a new or an existing node. The front then is updated, and the process continues until the entire region is meshed.

When generating a three-dimensional mesh, care must be taken to insure that the surface normals from each region point into the computational domain. Another potential difficulty occurs if the background mesh does not cover the entire flowfield domain. In this case, errors are produced when the front reaches the area not covered by the background grid. This especially can happen either if there are holes in the background grid or if somehow it is turned inside out.

FR3D / SWAN3D

The FR3D/SWAN3D package of programs, provided by Morgan and Peraire[4], is used to perform the meshing in two steps. FR3D creates the surface mesh, and

SWAN3D creates the flowfield mesh, using the output from FR3D as the initial front. These programs, specifically the surface mesh module, have several specific features which are discussed here. The first is that all lines are treated as splines. Generally, this is not a disadvantage, assuming that care is taken in specifying a sufficient number of points for the spline. Another feature is that there are three types of surfaces- planar, composite, and degenerate composite. Planar surfaces must be specified by their boundary segments and three points which define the normal to the plane.

Composite surfaces are specified by their boundary segments and by a surface spline which is used to map the physical space to two-dimensional space. One drawback is that this must be a one-to-one mapping, and this type of surface cannot be used for regions with singular points such as the nose of an aircraft. To handle these regions, degenerate composite surfaces are included to perform a simple triangularization of the boundary nodes and not create any nodes on the interior of that region. By using these three surface types, arbitrary geometries can be defined.

There are several advantages in using this package. The first is that because the surface splines are required, interior regions can be arbitrarily large, with little likelihood of loss of geometrical integrity. Another advantage is that new components can be added to an existing geometry with little difficulty. For example, pylons and stores can be added to the surface geometry without having to modify the existing wing data structure.

The FR3D/SWAN3D programs also have several disadvantages. Setup to work on mainframe computers, there is little in the way of a visual interface, so that it is often difficult to find trouble spots in the mesh. Another disadvantage is that the program has difficulty in generating meshes near regions of high curvature, such as the leading edge of many airfoils. Although used to generate a variety of meshes in

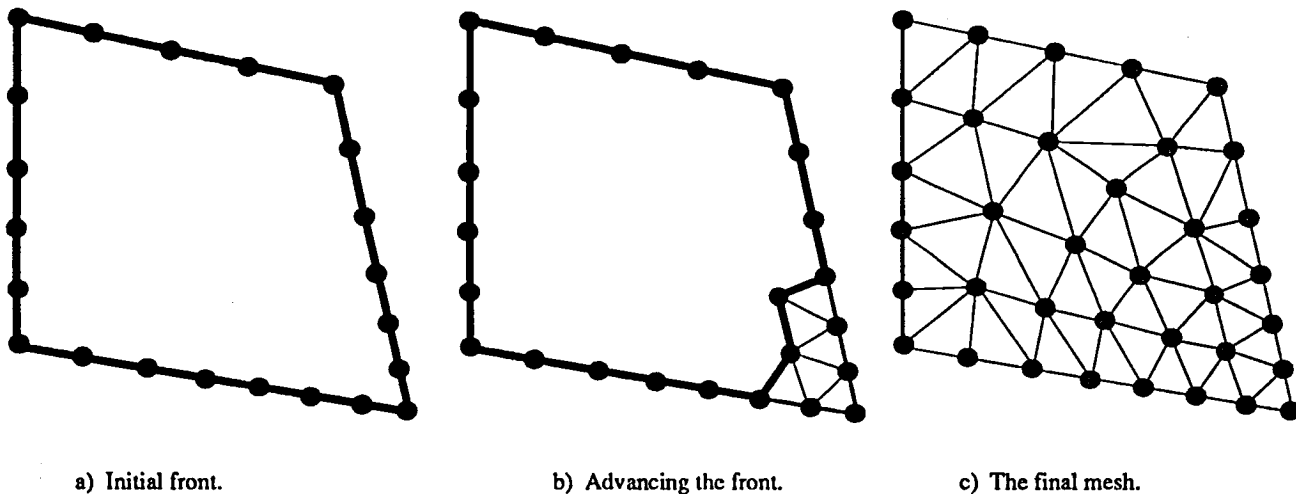


Figure 1. Advancing front method.

the early stages of the present study, none of the meshes were used in the calculations presented here.

VGRID3D

The VGRID3D package of programs, provided by Parikh, Pirzadeh, and Frink[15], takes a slightly different approach. The grid generation is done by one program; however there are several pre- and post- processing programs as well. Among them is a program to input the surface data, taken from existing structured data, graphically. Another pre-processing program is used to input data graphically and to make modifications to the background mesh.

This program treats three line types, including straight lines, parabolic lines, and arbitrary splined lines. There also are five kinds of surfaces, including planar, three and four segment parabolic, and three and four segment arbitrary surfaces. Using these different surfaces, it is possible to define arbitrary geometries.

A primary difference between the VGRID3D and SWAN3D codes is that while SWAN3D uses surface spline information, the VGRID3D program maps the information to and from computational space by solving the Poisson equation based on the boundary segments. For this reason, smaller surface regions must be used in VGRID3D in order that the interior geometry is not affected adversely.

Another difference is in the data format. For the FR3D code, the points that make up a line are defined along with the line. This leads to the duplication of endpoints in a list of input data, and for a complex geometry, can cause a noticeable increase in the size of a data file. For the VGRID3D code, all of the points that specify lines are given in one block, resulting in a more efficient data structure. This is a benefit if the data is being taken from a pre-existing data file. If points must be input by hand, however, this method is not necessarily the most error-free.

The greatest advantage of this program is the graphical interface. Written to run on a Silicon Graphics Iris Workstation, the program is able to display the surface mesh quickly from a variety of different locations, as well as being able to plot the front itself as it advances. In this way, the user can view the mesh as it is being created.

There are also disadvantages to using the VGRID3D program. One is that the input data is not modified easily. Adding elements to an existing data structure can require significant work. Because all non-planar surfaces must have either three or four segments as their boundaries, the addition of new components, such as stores or flaps, can increase greatly the number of surfaces, segments, and points required, not to mention the increased complexity of the data file itself.

Two-Dimensional Grid Quality

Grid qualities were defined first for two-dimensional meshes before investigating the quality of three-dimensional meshes. These two-dimensional qualities are described here briefly for simplicity. A complete set of two-dimensional mesh quality results may be found in reference [16].

Many quality measures can be devised for two-dimensional grids, but they generally all fall into two categories, individual element quantities and local or global mesh quantities. Individual element quantities are those which apply to elements by themselves, regardless of the surrounding mesh. Local quantities are those which apply to how an individual element "fits in" with the elements which surround it. These can be applied as local measures, if taken near an airfoil or other area of interest, or as global measures if taken over the entire mesh. One reason the parameters described below are chosen as two-dimensional quality measures is that they all can be extended readily to three dimensions.

Individual Element Quality

It is generally accepted that a mesh composed of equilateral triangles is ideal for two-dimensional unstructured meshes, just as a mesh composed of squares is ideal for structured meshes. Among individual element quantities, one that is in common use is a measure of the minimum angle of a triangle. By maximizing the minimum angle, an element becomes more uniform. By making use of the vector dot product, this quantity is reasonably simple to compute. It is not, however, the only measure of element quality.

A far less sophisticated method is to take the ratio of the maximum and minimum side lengths for each element. This is shown graphically in figure 2(a). This puts a bound on the minimum angle, but it requires less computation. In general, the extra computation required to determine the minimum angle itself is small. When these concepts are extrapolated to three-dimensions, however, small savings in individual computations can become significant.

Another way to measure element quality, shown in figure 2(b), is to define an aspect ratio for each element. This is defined by taking the ratio of the area of the smallest circle that can be superscribed about the triangle to the area of the largest circle that can be inscribed within the triangle. This measure then is normalized using the aspect ratio of an equilateral triangle, strictly for the sake of convenience, so that an aspect ratio of 1 indicates an equilateral triangle.

Local Mesh Quality

To measure local mesh qualities, information must be known about the neighboring elements. Because of the inherent random nature of unstructured grids, neighboring element information must also be known, resulting in additional

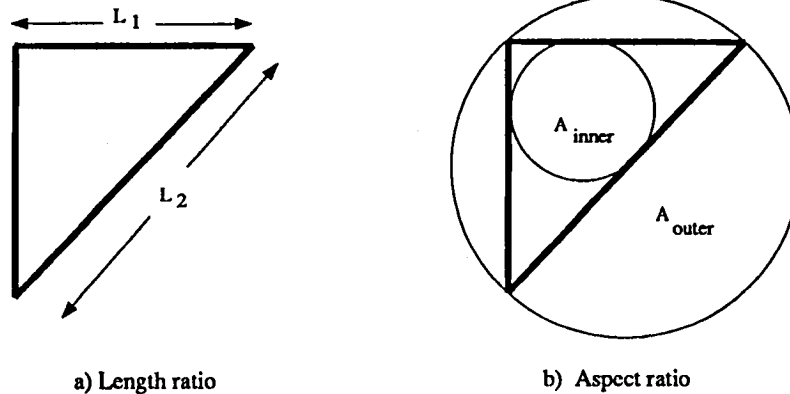


Figure 2. Definition of individual element quality parameters.

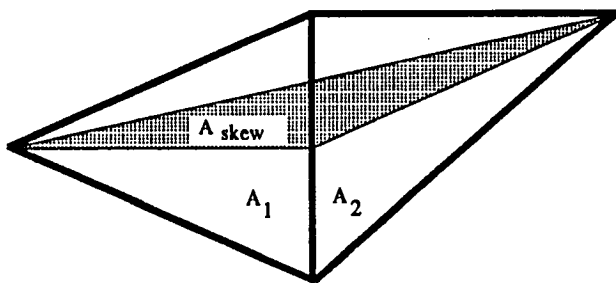


Figure 3. Area ratio and skewness definitions.

computational overhead. At the very minimum, the identity of the three triangles which surround a given triangle must be known. Additional nodal and connectivity information also are computed and stored for convenience.

Any of the above individual element quality measures also can be used as local mesh quality measures by taking ratios of their values across sides. For example, it might be advantageous to compare the aspect ratio of elements across edges. While these adapted measures can be useful, there are other local mesh quality measures which do not have individual element analogies. The most common of these is area ratios. These area ratios are useful to determine the amount of stretching in the mesh. For internal flow problems, such as ducts, this is not a great problem, but for external flows, such as airfoils, the stretching can be significant.

Another local quality measure is element skewness. A triangle can be formed using the midpoint of the side of interest and the two opposing vertices as shown in figure 3. The area of this triangle divided by the average area of the two base triangles gives the skewness across that face. This parameter is zero for a well-aligned mesh and, in general, will be less than one, except for highly-distorted meshes.

Three-Dimensional Grid Quality

The following subsections address individual element

quality and local mesh quality as they apply to three-dimensional grids.

Individual Element Quality

In three-dimensional meshes, the minimum angle measurement becomes the minimum dihedral angle measurement. The dihedral angle is measured using the vector dot product for each combination of the four faces which make up the tetrahedron. From this, the minimum of the six dihedral angles is found.

Another way to measure element quality is to take a ratio of the areas of the largest and smallest faces. The areas are found by taking the vector cross product of two of the three edges which make up a face. The magnitude of this vector is used as the area. This is far less computationally intensive than computing the dihedral angles for each face, and yields similar results.

An aspect ratio for a tetrahedron can be defined as the ratio of the volume of the smallest sphere that can surround the tetrahedron to the volume of the largest sphere that can be fit within the tetrahedron. This ratio then is normalized by the value of a "perfect" tetrahedron with equilateral faces.

There are other computations which can be made easily at the same time as other quality measures. One is an orientation checker. If the right hand rule is applied to all the faces in a tetrahedron, two faces will have normals which point inward, and two will have faces that point outward. Normally the connectivity information for these nodes is random, so checks must be made by the flow solver to determine which faces point inward and which point outward. If, however, all the nodes are arranged with the fourth node 'on top' of the first three, then the faces opposite the first and fourth nodes always will point inward, and the faces opposite the second and third nodes will point outward.

There also are local mesh quantities for three-dimensional meshes. These also require some information about the neighboring elements. As a minimum, the element numbers for the four neighbor elements must be known. If possible, it is beneficial to also store additional information, such as the neighboring element orientation or neighboring nodes. Also, as the two-dimensional quantities are measured across sides, the three-dimensional ones are measured across faces. Variations of the above individual element quantities can be measured across element faces, yielding some local quality measures.

In three dimensions, volume ratios are useful measures of stretching, just as area ratios are important in two dimensions. Mesh stretching is even more important in three dimensions than it is in two. This is because a doubling in the linear spacing will result in an eightfold increase in volume, and, consequently, large changes in the volume ratios are likely. These changes can be located with the volume parameter, indicating problems in the background grid.

Skewness measures also can be computed for three-dimensional elements. Using the two nodes on the opposite sides of the face of interest and the center of the face, a triangle is formed. The area of this triangle divided by the area of the face itself becomes the skewness. For two ideally aligned elements, the area of the formed triangle will be zero, resulting in zero skewness.

There are other problems with meshes in three dimensions which may be detected during quality assessment. One such problem with tetrahedral meshes is that it is very difficult to find elements with negative volume. These can occur after smoothing has been applied, or perhaps even by the grid generation program itself. One way to find these elements is to perform a global volume check. The absolute value of the volume of each of the elements is summed and compared to the expected volume enclosed by the boundaries. The problem with this method is that except for meshes with strictly defined outer boundaries, the expected volume is extremely difficult to compute. Even assuming it is calculable, the errors introduced potentially are greater than the volume of the element with negative area itself. Another problem with this method is that even if it works, it will only confirm the existence of a negative volume element. It is still up to the user to find that element. However, by comparing nodes across faces, it is possible not only to locate the presence of elements with negative volumes quickly and accurately, but to identify the elements themselves. For two adjoining elements with positive volume, their off nodes will be on opposite sides of the common face. For a combination of two elements, one of which has positive volume and the other which is distorted, these nodes will be on the same side of the common face. For a distorted mesh with two adjoining elements with negative volumes, this test will fail for this face but will pass for other faces of the distorted tetrahedron.

The inviscid flow about several unstructured two and three dimensional meshes was determined by solving the time-dependent Euler equations. The computational method is an implicit upwind flow solver that uses Roe's flux-difference splitting. The implicit temporal discretization is a two-sweep Gauss-Seidel relaxation procedure that is computationally efficient for either steady or unsteady flow problems. Details about the solution algorithm are given in reference [17].

Results

Calculations were performed to determine the quality of several unstructured meshes and to assess the accuracy of the flow solver by comparing calculations with experimental data. Three-dimensional results were obtained for two configurations for a variety of meshes and different flow conditions. Two ONERA M6 wing [18] cases were studied. The first case is for a freestream Mach number M_∞ of 0.699 and an angle of attack α of 3.06° which is hereafter referred to as case 1. The second calculation is at $M_\infty = 0.84$ and $\alpha = 3.06^\circ$ which is referred to as case 2. Additionally, meshes were generated about the Boeing 747 transport configuration, and a set of calculations were made. This is at $M_\infty = 0.70$ and $\alpha = 2.72^\circ$ which is referred to as case 3.

ONERA M6 Wing

To investigate spatial accuracy, results were obtained on three ONERA M6 wing meshes. This wing has been widely studied, and results have been obtained using many other flow solvers, on both structured and unstructured meshes. The wing has a leading edge sweep of 30° , an aspect ratio of 3.8, and a taper ratio of 0.56. It has a symmetrical cross section, a root chord of 0.6775, a semispan of 1.0, and a rounded tip. For this configuration, three meshes, the surface triangularizations of which are shown in figure 4, were generated. Sizes of these meshes are summarized in Table 1. These meshes are of increasing grid density to investigate the effects of mesh spacing on the calculated solution. Nodes are placed on these three meshes along the chord at the span stations $\eta = 0.2, 0.44, 0.6, 0.8, 0.9,$ and 0.95 to aid in making comparisons with the experimental pressure data of reference [18].

Mesh qualities for the ONERA M6 wing meshes are shown in figure 5. These assessment plots show the percentage of cells in each mesh which fall into certain quality ranges. For a uniform mesh of "ideal" tetrahedra, 100 percent of the cells would be in the leftmost columns. All three meshes were generated using the same mesh input data and background grid, with the only differences being in the global spacing parameter. Therefore it is not unexpected that the three meshes are of similar quality. It is worth noting that mesh quality improves as the mesh density increases,

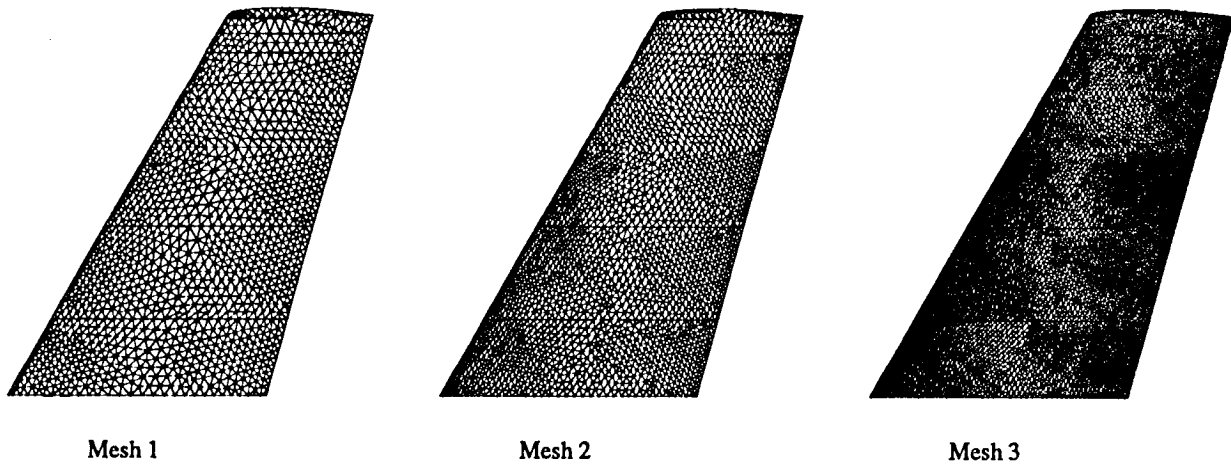


Figure 4. Surface triangularization for ONERA M6 wing meshes.

Table 1. Comparisons of ONERA M6 wing meshes.

	Mesh 1	Mesh 2	Mesh 3
Number of Cells	47,344	98,317	288,170
Number of Nodes	9,401	19,048	53,989
Number of Boundary Faces	5,860	10,388	23,164
Number of Boundary Nodes	2,932	5,196	11,584

suggesting that increases in grid density lead to more uniform cells.

Figure 6 shows coefficient of pressure comparisons with experimental data at several span stations for case 1. In these plots, coefficients of pressure computed using mesh 1 are denoted by the dashed line, coefficients of pressure on mesh 2 are given by the dotted line, coefficients of pressure on mesh 3 are given by the solid line, and experimental data is represented by the circles. The greatest effect of mesh density is near the leading edge, where the results obtained using mesh 3 show the best agreement with experiment. There is good agreement among the results for all three meshes aft of the 25 percent chord line, showing grid density has the greatest effect near the leading edge.

Convergence information for case 2 is shown in Table 2. This table shows the time required to achieve a four order of magnitude reduction in the L_2 -norm of the density residual, which was selected as the level for acceptable convergence.

Table 2. Convergence characteristics for ONERA M6 wing meshes for case 2.

	Mesh 1	Mesh 2	Mesh 3
CPU Time (Cray-2 minutes)	48	134	1,279
Iterations	998	1328	3258

For mesh 1, a converged solution was obtained in less than an hour of Cray-2 CPU time. For mesh 2, a converged solution was obtained in a little more than 2 hours of CPU time, while a solution on mesh 3 required about 20 hours. Coefficients of pressure are shown in figure 7. For this case, a double shock wave occurs on the upper surface of the wing and coalesces into a single, relatively strong shock near the wing tip. As is expected, coefficients of pressure for mesh 3 show the sharpest resolution of the double shock wave. Results for all three meshes show good agreement with each other aft of the 70 percent chord line on the upper surface, and aft of the 25 percent chord line on the lower surface. Pressure contours for this case are shown in figure 8 for the three meshes. The contours on all three meshes show the double shock wave on the upper surface. The contours on mesh 3 show much sharper shockwaves than the other two meshes, demonstrating an effect of mesh density. On the lower surface, there is less of a noticeable difference between the three sets of results.

Coefficients of lift, drag and pitching moment about the wing apex are given for the three meshes in Table 3.

These values were obtained by summing face centered values around the wing. Additionally the table presents lift, drag and moment values reported in reference [8] which were computed on a mesh with 231,507 elements

Table 3. Force and moment coefficients for ONERA M6 wing meshes.

	Mesh 1	Mesh 2	Mesh 3	Reference 8
Lift Coefficient	0.2892	0.2893	0.2923	0.2911
Drag Coefficient	0.0195	0.0167	0.0140	0.0123
Moment Coefficient	-0.1715	-0.1702	-0.1717	-0.1726

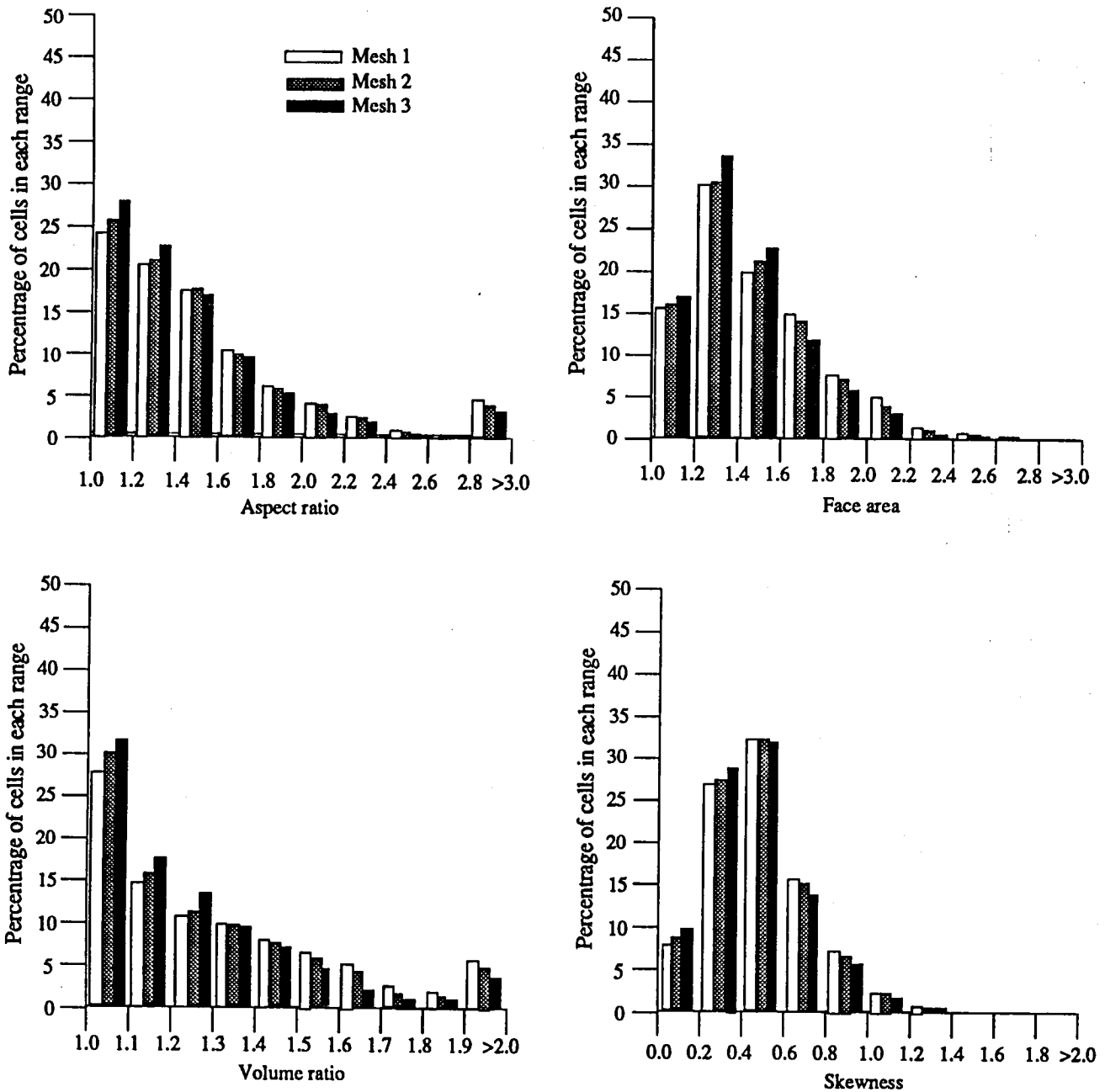


Figure 5. Comparison of mesh qualities for three ONERA M6 wing meshes.

and 16,984 nodes. This demonstrates good agreement between the present method and another unstructured upwind Euler solver.

Boeing 747 Transport

To investigate a more complex configuration, the Boeing 747 transport configuration was chosen. In addition to the wing and fuselage, this configuration includes flow-through engine nacelles and horizontal and vertical tails. Two meshes were generated for this configuration, the surface triangularizations of which are shown in figure 9. For

these meshes, the same surface input data was used, but different background grids were applied to achieve different density.

Mesh 1 is relatively coarse, with a finer mesh about the wing. Mesh 2 is an overall finer mesh, but is coarser over the wing. Table 4 presents a summary of the mesh sizes. While mesh 2 has nearly twice the number of cells of mesh 1, mesh 2 has only a 24 percent more boundary faces. Mesh qualities are given for the two meshes in figure 10. Based on the quality evaluations, mesh 2 is of higher quality than mesh 1, which is expected due to the more uniform nature

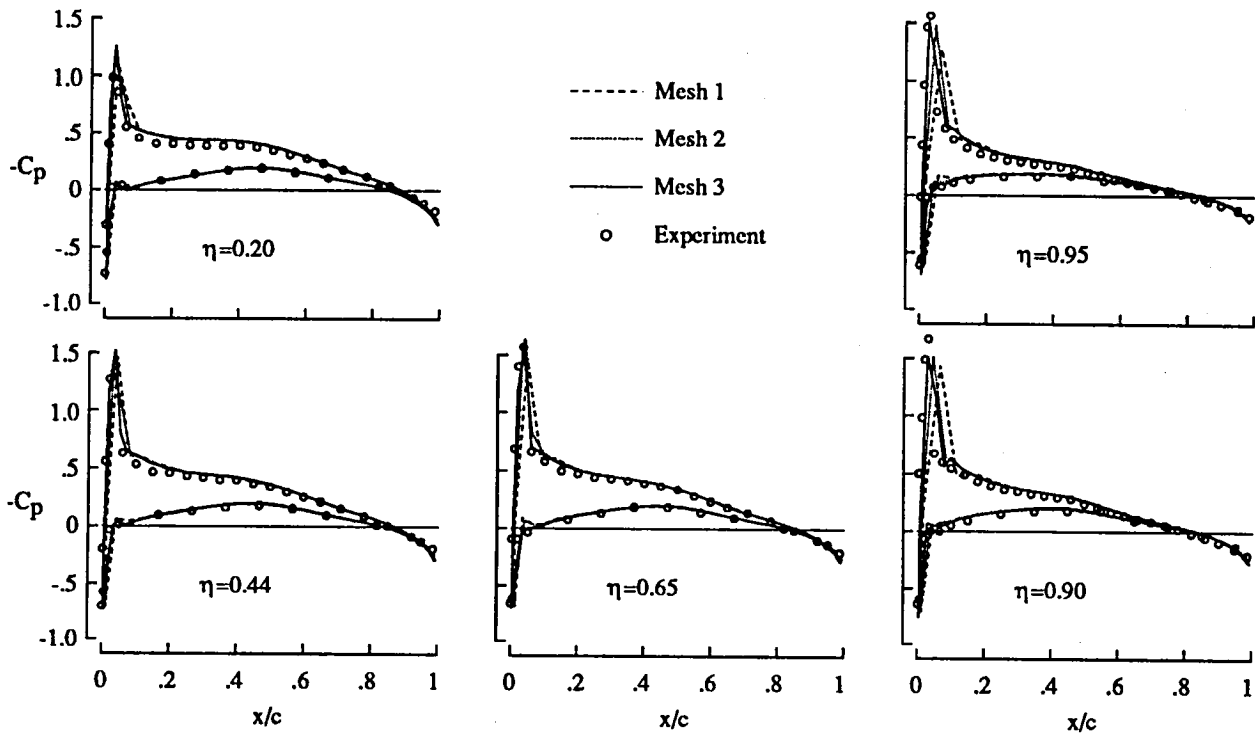


Figure 6. Comparison of calculated and measured coefficients of pressure on the ONERA M6 wing at $M_\infty = 0.699$ and $\alpha = 3.06^\circ$.

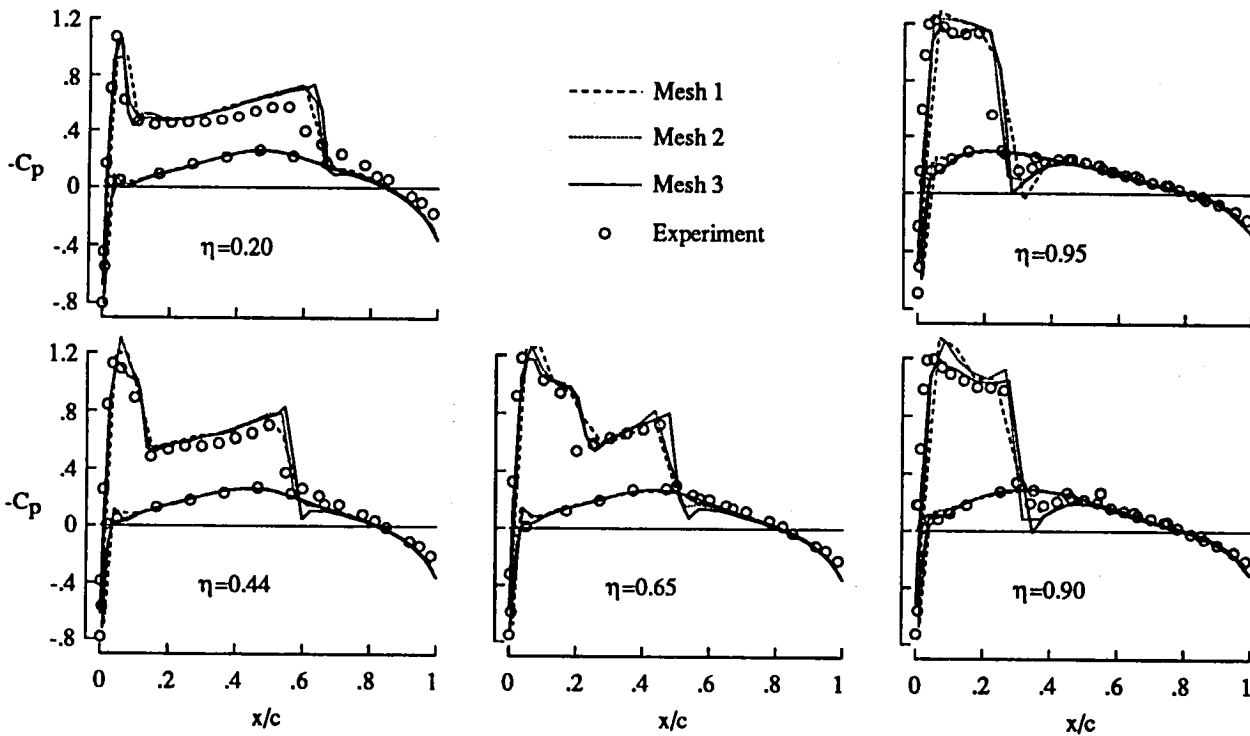


Figure 7. Comparison of calculated and measured coefficients of pressure on the ONERA M6 wing at $M_\infty = 0.84$ and $\alpha = 3.06^\circ$.

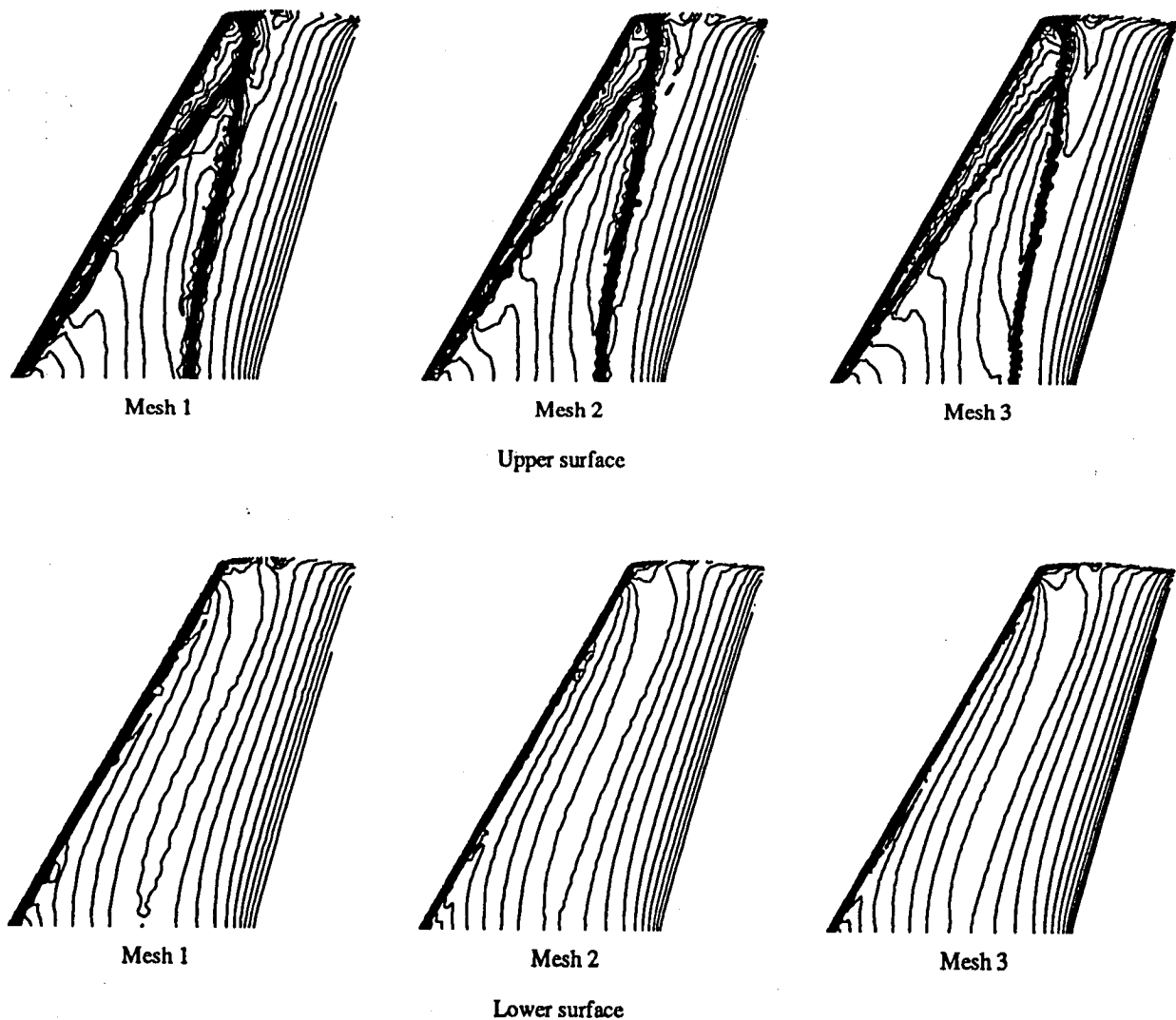


Figure 8. Surface pressure contours on the ONERA M6 wing for three meshes, $M_\infty = 0.84$ and $\alpha = 3.06^\circ$ ($\Delta P/P_\infty = 0.02$).

Table 4. Comparisons of Boeing 747 transport configuration meshes.

	Mesh 1	Mesh 2
Number of Cells	138,546	216,864
Number of Nodes	26,040	39,847
Number of Boundary Faces	11,460	14,254
Number of Boundary Nodes	5,724	7,121

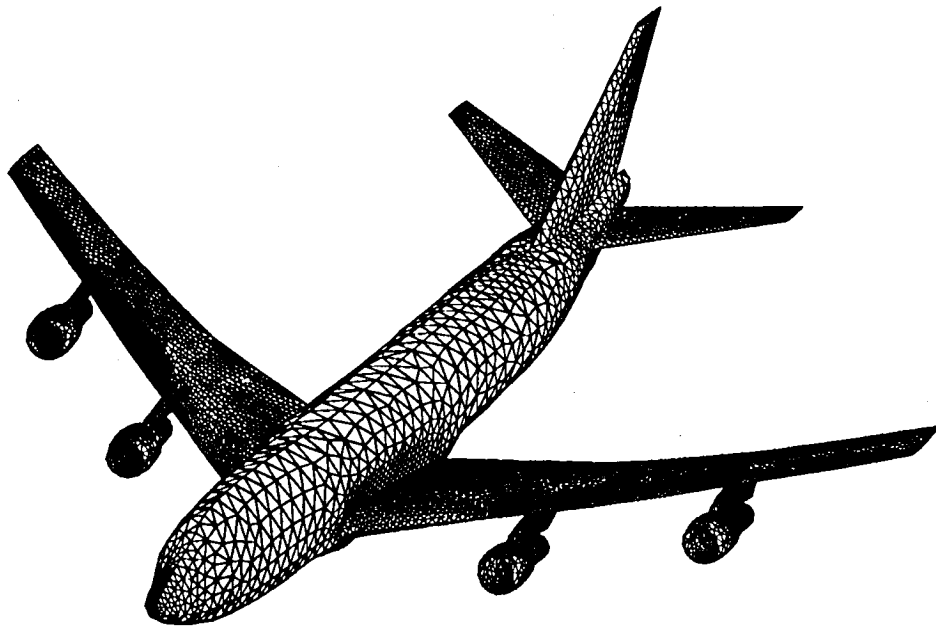
of the mesh.

Coefficients of pressure for case 3 on the wing at several span stations are shown in figure 11, along with experimental data. Values for mesh 1 are given by the solid and values for mesh 2 are given by dashed lines. Calculations

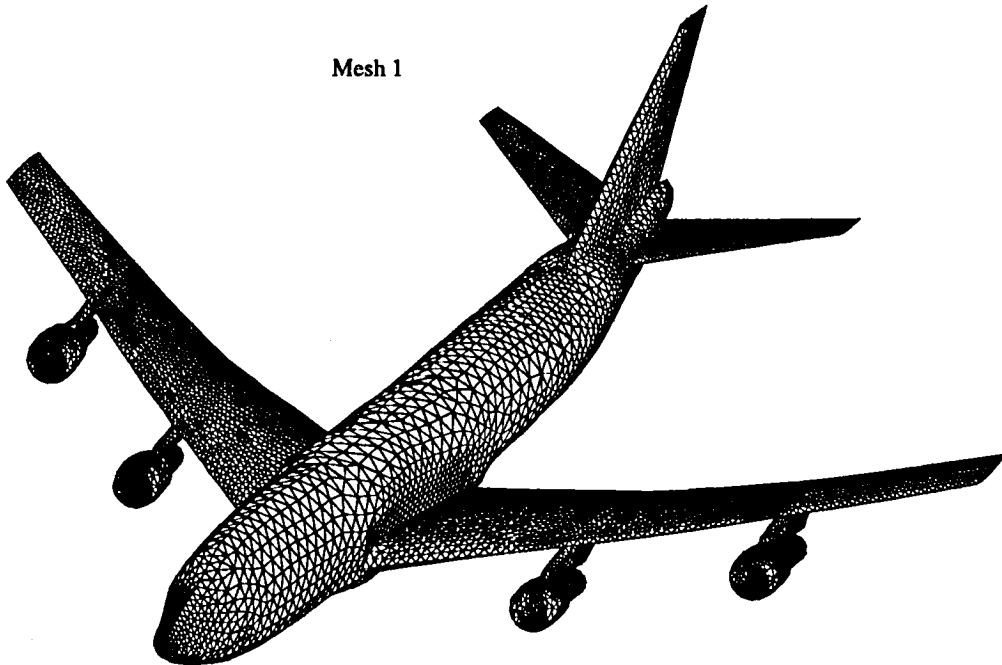
show reasonable agreement with experimental data. Results obtained on mesh 1 are in slightly better agreement with the experimental values, because the mesh 1 is actually finer over most of the wing, while mesh 2 is globally finer but coarser over the wing. These differences are believed to be a direct result of mesh coarseness, and not an indication of deficiencies in the flow solver. Meshes of higher density are being used to resolve these inconsistencies. Pressure contours about the entire aircraft for mesh 2 are shown in figure 12. The lighter regions indicate areas of high pressure, while the darker regions are those with lower pressure.

Concluding Remarks

Quality assessment procedures were described for two-dimensional and three-dimensional unstructured meshes. The procedures include measurement of minimum angles,



Mesh 1



Mesh 2

Figure 9. Surface triangularization of two Boeing 747 transport configuration meshes.

element aspect ratios, stretching, and element skewness. Meshes about the ONERA M6 wing and the Boeing 747 transport configuration were generated using an advancing front method grid generation package, and qualities of these meshes were assessed.

Validation of an implicit upwind Euler solution algorithm was begun by obtaining solutions of Euler's equations

for these meshes at low angle of attack, transonic conditions. Results for these cases demonstrated the accuracy of the current solution algorithm. Comparisons of calculated pressures with experimental data show excellent agreement for the ONERA M6 wing meshes. Similar comparisons of calculated pressures with experimental data for the 747 configuration show reasonable agreement.

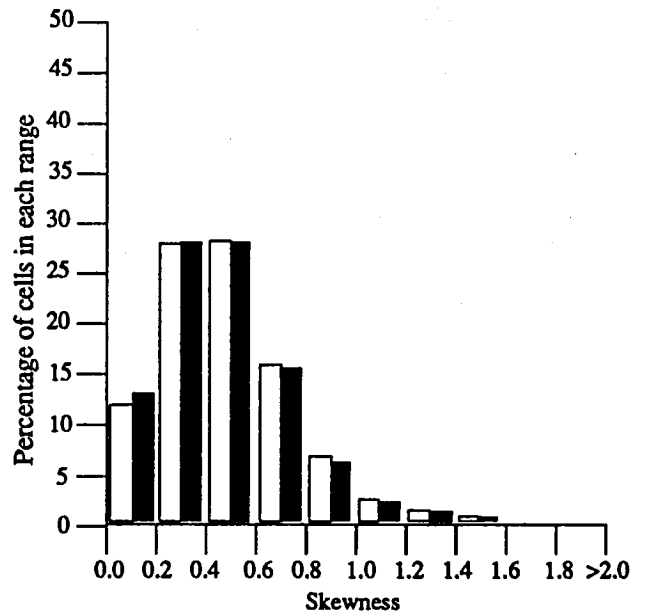
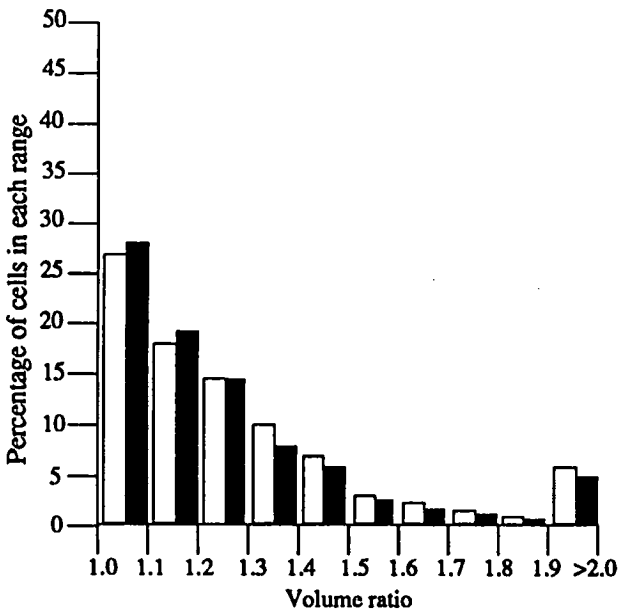
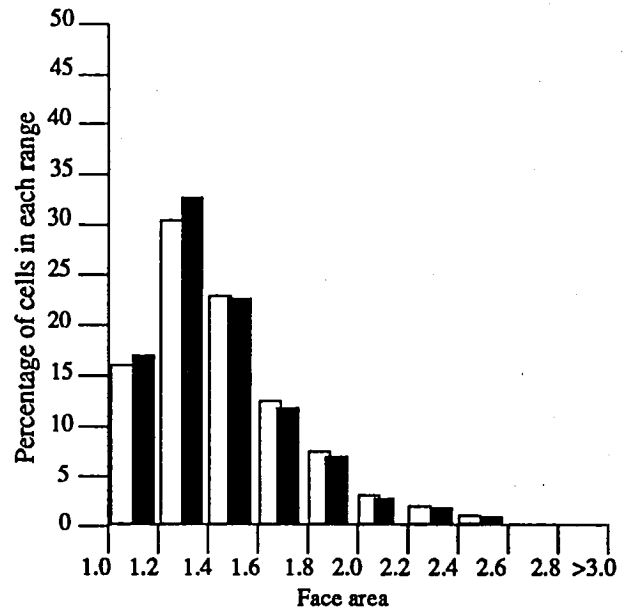
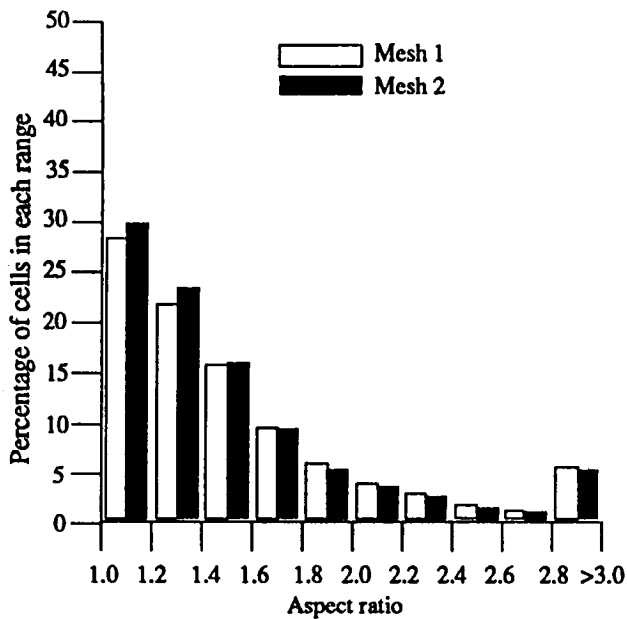


Figure 10. Comparisons of mesh quality for two Boeing 747 transport configuration meshes.

Acknowledgments

The work constitutes a part of the first author's M.S. thesis at Purdue University and was supported by the NASA Langley Graduate Aeronautics Program under grant NAG-1-372. The authors acknowledge Ken Morgan of the University College of Swansea, U.K. and Jaime Peraire of the Imperial College of Science, Technology, and Medicine, London, England, for providing the FR3D/SWAN3D software. Additionally the authors acknowledge Paresh Parikh and Shahyar Pirzadch of ViGYAN Inc., Hampton, Virginia,

and Neal Frink of the Transonic Aerodynamics Branch at NASA Langley Research Center, Hampton, Virginia, for providing the VGRID3D software which was used to create the ONERA M6 wing and the Boeing 747 transport configuration meshes in the present study.

References

- 1 Jameson, A., Baker, T. J., and Weatherill, N. P. : Calculation of Inviscid Transonic Flow Over a Complete Aircraft. AIAA-86-0103, January 1986.

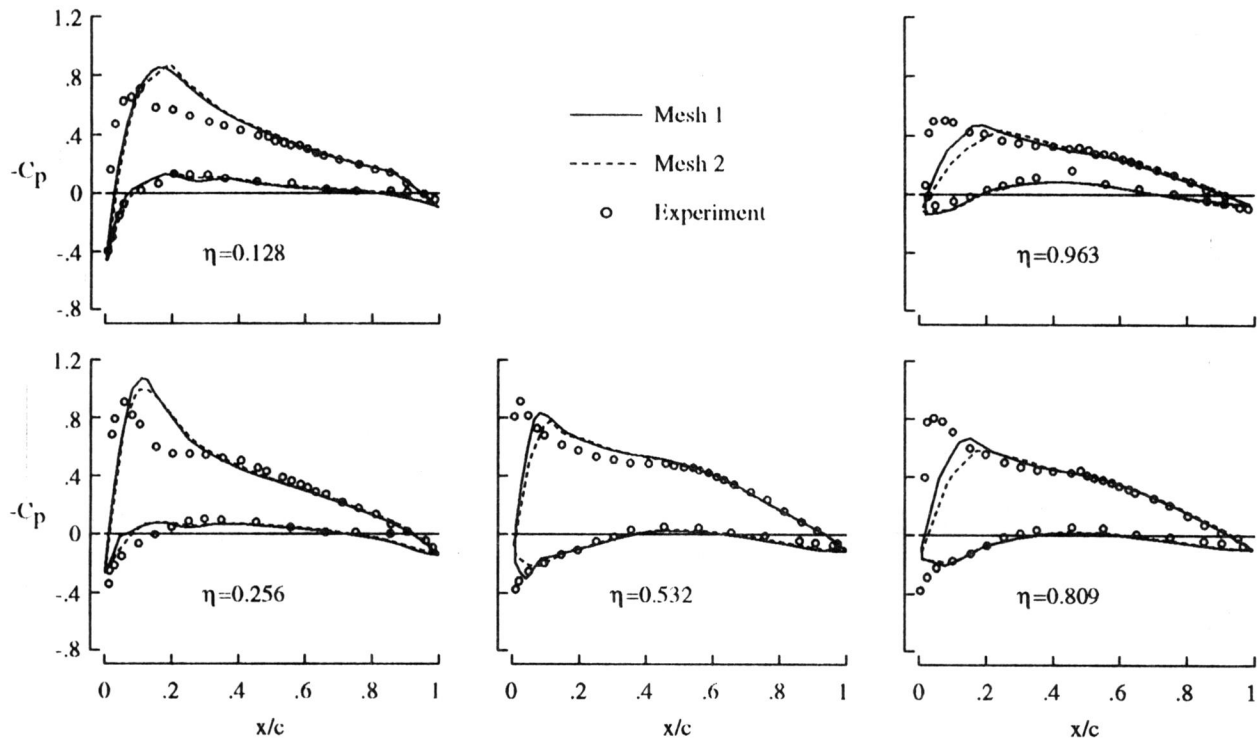


Figure 11. Comparison of calculated and measured coefficients of pressure on the Boeing 747 transport configuration at $M_\infty = 0.7$ and $\alpha = 2.72^\circ$.

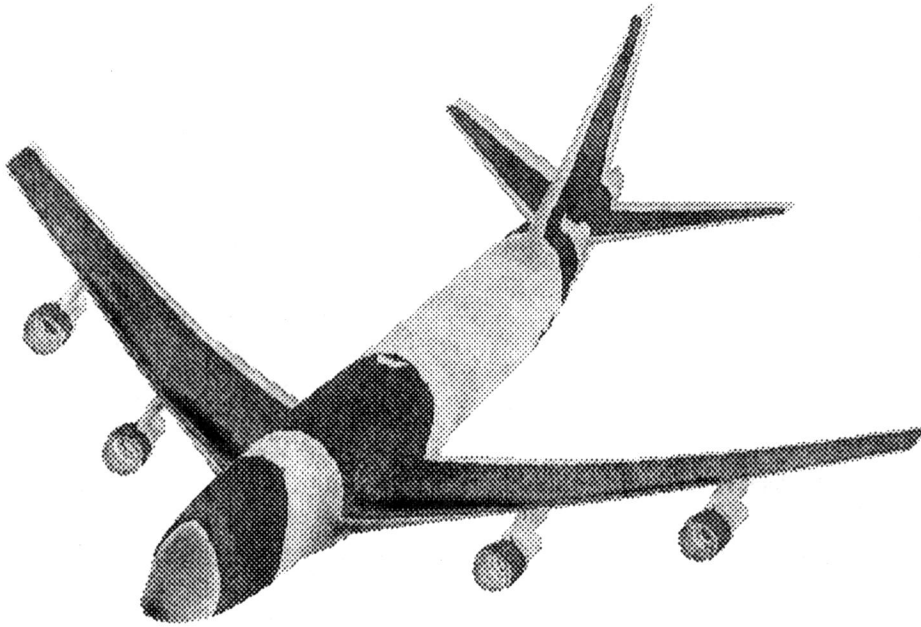


Figure 12. Pressure contours on a Boeing 747 transport configuration computed using mesh 2 at $M_\infty = 0.7$ and $\alpha = 2.72^\circ$.

- ² Mavriplis, D. and Jameson, A. : Multigrid Solution of the Two-Dimensional Euler Equations on Unstructured Triangular Meshes. AIAA-87-0353, January 1987.
- ³ Rausch, R.D., Batina, J.T. and Yang, H. T. Y. : Euler Flutter Analysis of Airfoils Using Unstructured Dynamic Meshes. AIAA-89-1384, April 1989.
- ⁴ Peraire, J., Morgan, K. and Peiro, J. : Unstructured Finite Element Mesh Generation and Adaptive Procedures

for CFD. AGARD-CP-464, May 1989.

- ⁵ Batina, J.T. : Accuracy of an Unstructured-Grid Upwind-Euler Algorithm for the ONERA M6 Wing, January 17-18 1990. Presented at the Accuracy of Unstructured Grid Techniques Workshop. NASA Langley Research Center, Hampton, Virginia.
- ⁶ Kleb, W. L., Batina, J.T., and Williams, M. H. : Temporal Adaptive Euler/Navier-Stokes Algorithm for

- Unsteady Aerodynamic Analysis of Airfoils Using Unstructured Dynamic Meshes. AIAA-90-1650, June 1990.
- 7 Rausch, R.D., Batina, J.T. and Yang, H. T. Y. : Spatial Adaption Procedures on Unstructured Meshes for Accurate Unsteady Aerodynamic Flow Computation. AIAA-91-1106, April 1991.
 - 8 Frink, N. T., Parikh, P., and Pirzadeh, S. : A Fast Upwind Solver for the Euler Equations on Three-Dimensional Unstructured Meshes. AIAA-91-0102, January 1991.
 - 9 Frink, N. T., Parikh, P., and Pirzadeh, S. : Aerodynamic Analysis of Complex Configurations Using Unstructured Grids. AIAA-91-3292, September 1991.
 - 10 Watson, D. F. : Computing the N-Dimensional Delaunay Tessellation with Application to Voronoi Polytopes. *The Computer Journal*, 24(2), 1981. pp. 167-172.
 - 11 Sloan, S.W. and Houlshy, G.T. : An Implementation of Watson's Algorithm for Computing 2-Dimensional Delaunay Triangulations. *Adv. Eng. Software*, 6(4), 1984. pp. 192-197.
 - 12 Tanemura, M., Ogawa, T. and Ogita, N. : A New Algorithm for Three-Dimensional Voronoi Tessellation. *Journal of Computational Physics*, 51, 1983. pp. 191-207.
 - 13 Baker, T.J. : Three Dimensional Mesh Generation by Triangulation of Arbitrary Point Sets. AIAA-87-1124-CP, 1987.
 - 14 Löhner, R. and Parikh, P. : Generation of Three-Dimensional Unstructured Grids by the Advancing Front Method. *International Journal of Numerical Methods Fluids*, 8, 1988. pp. 1135-1149.
 - 15 Parikh, P., Pirzadeh, S. and Löhner, R. : A Package for 3-D Unstructured Grid Generation, Finite-Element Flow Solution and Flow Field Visualization. NASA CR-182090, September 1990.
 - 16 Woodard, P. R. : Grid Quality Assessment for Unstructured Triangular and Tetrahedral Meshes. Master's thesis, Purdue University, 1992.
 - 17 Batina, J. T. : A Fast Implicit Upwind Solution Algorithm for Three Dimensional Unstructured Dynamic Meshes. AIAA-92-0447, January 1992.
 - 18 Schmidt, V. and Charpin, F. : Pressure Distributions on the ONERA M6 Wing at Transonic Mach Numbers, May 1979. Appendix B1 in AGARD-AR-138, Experimental Data Base for Computer Program Assessment.

